NORGES TEKNISK-NATURVITENSKAPELIGE
UNIVERSITET

A nonlinear dynamic finite strain formulation of an elastic pipe during pipeline installation

by

G.A. Jensen, N. Säfström, T.D. Nguyen and T. I. Fossen

PREPRINT
NUMERICS NO. 8/2008

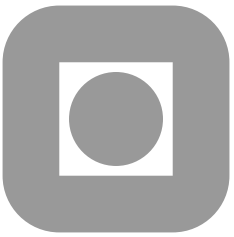

NORWEGIAN UNIVERSITY OF
SCIENCE AND TECHNOLOGY
TRONDHEIM, NORWAY

This report has URL
http://www.math.ntnu.no/preprint/numerics/2008/N8-2008.pdf
Address: Department of Mathematical Sciences, Norwegian University of Science and Technology, N-7491 Trondheim, Norway.

A nonlinear dynamic finite strain formulation of an elastic pipe during pipeline installation

G.A. Jensen, N. Säfström, T.D. Nguyen and T. I. Fossen

October 16, 2008

In this paper a nonlinear finite shear pipe formulation for freely suspended offshore pipes completely submerged in water is developed.

A Nonlinear Dynamic Finite Strain Formulation of an Elastic Pipe During Pipeline Installation

Gullik A. Jensen[a,*], Niklas Säfström[b], Tu Duc Nguyen[c], Thor I. Fossen[a,d]

[a] *Department of Engineering Cybernetics, Norwegian University of Science and Technology, NO-7491 Trondheim, Norway*
[b] *Department of Mathematical Sciences, Norwegian University of Science and Technology, NO-7491 Trondheim, Norway*
[c] *Siemens Oil & Gas Offshore, NO-7037 Trondheim, Norway*
[d] *Centre for Ships and Ocean Structures, Norwegian University of Science and Technology, NO-7491 Trondheim, Norway*

Abstract

In this paper a nonlinear finite shear pipe formulation for a freely suspended offshore pipe completely submerged in water is developed. The pipe model is three-dimensional and capable of undergoing finite extension, shearing, twist and bending. The formulation is well suited for simulation and control applications. The pipe extends from a surface vessel to the seabed. A potential theory formulation of a surface vessel suited for dynamic positioning and low speed manoeuvring is used as the upper boundary condition. The stability properties of the system is established. The pipe formulation is shown to be energy dissipating, and the total system is shown to be input-output passive, taking the vessel thrusters as input and the velocity vector as output. A numerical implementation based on the finite element method is presented along with simulation results that are in agreement with the theoretical results.

Key words: Pipeline installation, modeling, nonlinear, passivity, simulation, FEM

1. Introduction

The unprecedented global demand for oil and gas, coupled with the high commodity prices, drives the demand for pipelines in the offshore petroleum industry. Even more, the pipelines are required to be longer, larger and at deeper water depths then ever before. Mathematical models are essential in the design, installation and operation of pipelines. The motivation for this work is to develop a pipemodel suitable for simulating the freely suspended pipe in a pipeline installation operation. The dynamic behavior of the pipe model should be as close to a "real-world" pipe as possible. This implies that the model needs to be three-dimensional and include finite extension, shearing, twist and bending. A continuous model is considered rather than a discrete one, as it yields a better system understanding. The stability properties of a continuous system are more easily found, and may directly be imposed on the discretization done in implementing the model. When the stability of the pipe model has been shown, it becomes applicable for designing model based automatic controllers. The advantages gained

*Corresponding author
Email addresses: gullik.jensen@itk.ntnu.no (Gullik A. Jensen), niklas.savstrom@math.ntnu.no (Niklas Säfström), tu.nguyen@siemens.com (Tu Duc Nguyen), fossen@ieee.org (Thor I. Fossen)

in a pipeline installation operation by using an automatic control system, computing an optimal path and speed for the vessel, are increased accuracy and lay rates. Equipped with a suitable pipemodel, the implementation of an automatic control system is limited to a software extension of the dynamical positioning (DP) system, which has already become common practice in pipeline installation. The model is valid for any kind of slender marine structure suspended freely in water such as pipelines, cables, umbilicals, mooring lines, flexible and stiff risers. However the authors have chosen to limit the study to a pipeline being installed from a surface vessel.

1.1. Mathematical Models

The catenary equation has been known for centuries, and it was used in modeling the pipelay operation in its infancy. This equation is extensively treated by Irvine (1981). The catenary equation does not account for bending stiffness, and an extension was made to amend this deficiency by Plukett (1967) and Dixon and Rutledge (1968). Today, the method of choice to simulate pipes and similar structures are computer tools such as ABAQUS, OFFPIPE, RIFLEX and SIMLA, which are based on discrete finite element models. These models are constructed by joining predefined beam or bar elements to a complete structure. Finite element models are versatile, and high quality discrete dynamic models can be obtained without exact knowledge of the modeled system. Modeling and simulation of a pipelay using ABAQUS is found in (Martinsen, 1998). Proving stability of a finite element model is difficult. However, if a system of partial differential equations (PDE) of the pipe is known, the stability can be proven for this system. Discretization of this continuous system using the finite element method (FEM) yields a semi discrete finite element model that is suited for simulations and inherits the stability properties of the continuous system. The key feature of the model developed in this paper is the choice of parametrization which yields a continuous momentum equation on a form which strongly resembles the classical Euler equation of rigid body dynamics. It is well suited for both mathematical and numerical analysis. The high complexity of finite element models makes it unsuited for closed loop automatic control. For this reason simpler models that contains the main dynamics only, such as (Jensen et al., 2008) based on the robot equation, has been preferred for feed-back control applications.

1.2. Model Based Controllers

Mechanical flexible systems are continuous, and in theory infinite-dimensional. In practice these systems are modeled as finite-dimensional with a large number of dimensions. The fundamental problem of actively controlling very flexible systems is to control a large-dimensional system with a much smaller dimensional controller. This topic was addressed as early as in the 1970's by Balas (1978). It shows that controllers based on finite dimensional models can become unstable when connected to infinite-dimensional systems. This is due to the unmodeled modes in the system, named *the spillover*, which the controller does not account for. An unstable control system may cause disastrous behavior. In this paper the stability of the developed pipemodel is shown. A controller based on this model can thus be shown to be stable, such that the closed loop system is stable and the disastrous effects are avoided.

2. Mathematical Model

A nonlinear finite shear pipe formulation for a freely suspended offshore pipe completely submerged in water is developed in this section. The model of the pipe dynamics is a partial differential equation extending the nonlinear finite shear beam formulation developed and investigated by Simo et al. in a series of papers published in the mid and late 1980s (Simo, 1985; Simo and Vu-Quoc, 1986, 1988; Simo et al., 1995). The formulation is a three-dimensional generalization of the formulation originally developed by Reissner (1982). This model again can be regarded as a convenient parametrization of a three-dimensional extension of the classical Kirchhoff-Love rod model (Love, 1944). The extension includes finite extension and finite shearing of the rod. In this paper the hydrodynamic and hydrostatic effects caused by the marine environment is accounted for. The model is developed for low speed applications such as pipe line installation and risers, which implies that the hydrodynamic drag will dominate the added mass terms. Thus it is a reasonable assumption to neglect the acceleration term of the damping.

The pipe extends from a surface vessel and down to the seabed, which gives rise to the boundary conditions. A vessel model in the time domain, suitable for low speed manoeuvring and station keeping, is taken as the upper boundary condition. The vessel model is obtained by considering the forces and moments on a rigid body as well as hydrodynamic radiation forces and wave loads. The dynamic vessel model is a system of ordinary differential equations in the time domain and state space.

In this section, the notation and reference frames are introduced, followed by the kinematics and the dynamic pipe model with boundary conditions.

2.1. Notation

Bold face lower and upper case letters denote vectors and matrices respectively. A superscript denote the reference frame of coordinate vectors. This may be omitted if the frame dependency is evident. The derivative with respect to time is denoted by a superposed dot, and the material derivative is denoted by a prefixed ∂_S. The usual inner product of $\boldsymbol{a}, \boldsymbol{b} \in \mathbb{R}^n$ is denoted $\langle \boldsymbol{a}, \boldsymbol{b} \rangle$ or equivalently $\boldsymbol{a}^{\mathrm{T}}\boldsymbol{b}$.

2.2. Model Preliminaries

The pipe is in a classical point of view a rod, which is a three-dimensional body whose reference configuration can be described by a smooth curve $\boldsymbol{\varphi}_r$, which at each point has attached a cross-section plane (Figure 1). The tangent of the curve $\boldsymbol{\varphi}_r$ is assumed to be normal to each cross-section, intersecting at the centroid. Any configuration of the pipe is thus given by a smooth curve $\boldsymbol{\varphi} : [0, L] \to \mathbb{R}^3$ denoted the *line of centroids*. L is the total length of the undeformed beam reference configuration $\boldsymbol{\varphi}_r$. The cross-sections are assumed to remain unchanged in shape but not necessarily remain normal to the tangent $\partial_S \boldsymbol{\varphi}$ (shearing), while the beam is undergoing motion, which is the case for the Euler-Bernoulli beam. The position of any point on the line of centroid is given by $\boldsymbol{\varphi}(S)$ and the orientation of the cross-section at $\boldsymbol{\varphi}(S)$ is given by the rotation matrix $\boldsymbol{R}_t^e(S)$. Thus the configurations of the pipe are completely defined by specifying the evolution of the position vector of the line of centroids $\boldsymbol{\varphi}(S, t)$

and the orthogonal rotation matrix $\boldsymbol{R}_t^e(S,t)$ along the material variable S. The configuration space for the elastic pipe is

$$\mathcal{C} = \left\{ (\boldsymbol{\varphi}, \boldsymbol{R}_t^e) \,|S \in [0,L] \rightarrow \mathbb{R}^3 \times SO(3) \,|\, \langle \partial_S \boldsymbol{\varphi}(S), \boldsymbol{R}_t^e \boldsymbol{e}_1^e \rangle > 0 \right\} \tag{1}$$

The reference configuration is taken as $(\boldsymbol{\varphi}_r, \boldsymbol{R}_{t,r}^e) \in \mathcal{C}$ such that

$$\boldsymbol{\varphi}_r(S) = S\boldsymbol{e}_1^e, \quad \boldsymbol{R}_{t,r}^e(S) = \boldsymbol{I}_{3\times 3}. \tag{2}$$

2.3. Reference Frames

Three orthonormal reference frames $\boldsymbol{e}$, $\boldsymbol{t}$ and $\boldsymbol{b}$ are used in this paper as illustrated in Figure 2. Let $\boldsymbol{e}$ be an inertial frame with origin O_e and base $\boldsymbol{e}_1, \boldsymbol{e}_2, \boldsymbol{e}_3$, called the *spatial* frame. Let O_e be fixed at the seabed and at the base of the pipe ($S = 0$). Let $\boldsymbol{t}(S)$ be a moving frame with base $\boldsymbol{t}_1(S), \boldsymbol{t}_2(S), \boldsymbol{t}_3(S)$, with $\boldsymbol{t}_2(S)$ and $\boldsymbol{t}_3(S)$ directed along the principal axis of the cross-section plane, and $\boldsymbol{t}_1(S)$ normal to the plane in order to form a right-hand system. The origin $O_t(S)$ is located at point $\boldsymbol{\varphi}(S)$ on the centroid. This frame is called the *material* frame. Let $\boldsymbol{b}$ with basis $\boldsymbol{b}_1, \boldsymbol{b}_2, \boldsymbol{b}_3$ with origin O_b in the mass center of the vessel, oriented in accordance with (SNAME, 1950), be denoted the body fixed frame. The three rotation matrices

$$\boldsymbol{R}_t^e(S), \boldsymbol{R}_b^e, \boldsymbol{R}_b^t \in SO(3) \tag{3}$$

are respectively defined for $i = 1, 2, 3$ as

$$\boldsymbol{t}_i^e(S) = \boldsymbol{R}_t^e(S)\boldsymbol{e}_i^e, \quad \boldsymbol{b}_i^e = \boldsymbol{R}_b^e \boldsymbol{e}_i^e, \quad \boldsymbol{b}_i^t = \boldsymbol{R}_b^t \boldsymbol{t}_i^t. \tag{4}$$

Matrix $\boldsymbol{R}_t^e$ denotes the rotation from $\boldsymbol{e}$ to $\boldsymbol{t}$ and the coordinate transformation from $\boldsymbol{t}$ to $\boldsymbol{e}$, and equally for $\boldsymbol{R}_b^e$ and $\boldsymbol{R}_b^t$. Noting that a rotation matrix of composite rotations is the product of rotation matrices, $\boldsymbol{R}_b^e$ can be found to be

$$\boldsymbol{R}_b^e = \boldsymbol{R}_t^e(L)\boldsymbol{R}_b^t. \tag{5}$$

2.4. Kinematics

In this section the derivatives with respect to time t and space S of $\boldsymbol{\varphi}(S,t)$ and $\boldsymbol{R}_t^e(S,t)$ required in the pipe equations of motion are found. The material stress resultant and stress couple are presented.

2.4.1. Time Derivatives

Differentiating equation (4) with respect to time t yields

$$\dot{\boldsymbol{t}}_i^e = \boldsymbol{S}(\mathbf{w}^e)\boldsymbol{t}_i^e, \quad \boldsymbol{S}(\mathbf{w}^e) = \dot{\boldsymbol{R}}_t^e (\boldsymbol{R}_t^e)^{\mathrm{T}} \tag{6}$$

where $\boldsymbol{S}(\mathbf{w}^e(S,t))$ is a skew-symmetric tensor field that defines the *spin* of the moving frame, and the associated axial vector $\mathbf{w}^e(S,t)$ defines the *vorticity*. $\boldsymbol{S}(\cdot) : \mathbb{R}^3 \rightarrow T_I SO(3)$ is the skew-symmetric operator. The time derivative of the rotation matrix is given by the two forms

$$\dot{\boldsymbol{R}}_t^e = \boldsymbol{R}_t^e \boldsymbol{S}(\mathbf{w}^t) \tag{7}$$

$$\dot{\boldsymbol{R}}_t^e = \boldsymbol{S}(\mathbf{w}^e)\boldsymbol{R}_t^e. \tag{8}$$

The linear velocity vector is given in the spatial and material frames respectivly as

$$\dot{\boldsymbol{\varphi}} \in \mathbb{R}^3, \qquad \boldsymbol{v}^t = \left(\boldsymbol{R}_t^e\right)^{\mathrm{T}} \dot{\boldsymbol{\varphi}}. \tag{9}$$

By differentiating equation (9), the linear acceleration in the two frames becomes

$$\ddot{\boldsymbol{\varphi}} \in \mathbb{R}^3, \qquad \dot{\boldsymbol{v}}^t = \left(\boldsymbol{R}_t^e\right)^{\mathrm{T}} \ddot{\boldsymbol{\varphi}} - \left(\boldsymbol{R}_t^e\right)^{\mathrm{T}} \left[\mathbf{w}^e \times \dot{\boldsymbol{\varphi}}\right]. \tag{10}$$

2.4.2. Space Derivatives

The material derivative of the position vector is denoted $\partial_S \boldsymbol{\varphi}\left(S,t\right) \in \mathbb{R}^3$. The derivative with respect to S of the rotation matrix is, like the time derivative, obtained from differentiating equation (4). The kinematic differential equations of the rotation matrix is given by the two alternative forms:

$$\partial_S \boldsymbol{R}_t^e = \boldsymbol{R}_t^e \boldsymbol{S}\left(\boldsymbol{\omega}^t\right) \tag{11}$$

$$\partial_S \boldsymbol{R}_t^e = \boldsymbol{S}\left(\boldsymbol{\omega}^e\right) \boldsymbol{R}_t^e. \tag{12}$$

where

$$\boldsymbol{S}\left(\boldsymbol{\omega}^t\right) = \partial_S \left(\boldsymbol{R}_t^e\right) \left(\boldsymbol{R}_t^e\right)^{\mathrm{T}}. \tag{13}$$

The difference of the spatial derivative of (7) and the time derivative of (11) yields the equation

$$\dot{\boldsymbol{\omega}}^t = \partial_S \mathbf{w}^t + \boldsymbol{\omega}^t \times \mathbf{w}^t = \left(\boldsymbol{R}_t^e\right)^{\mathrm{T}} \left[\partial_S \mathbf{w}^e + \boldsymbol{\omega}^e \times \mathbf{w}^e\right], \tag{14}$$

that relates $\boldsymbol{\omega}$ and $\mathbf{w}$, which will be needed in the stability proof.

2.4.3. Stress

The material stress resultant $\boldsymbol{n}^t$ and stress couple $\boldsymbol{m}^t$ are obtained from the bilinear quadratic energy function $\boldsymbol{\Psi}(\boldsymbol{\gamma}^t, \boldsymbol{\omega}^t)$ (Simo, 1985),

$$\boldsymbol{n}^t = \frac{\partial}{\partial \boldsymbol{\gamma}^t} \boldsymbol{\Psi}, \quad \boldsymbol{m}^t = \frac{\partial}{\partial \boldsymbol{\omega}^t} \boldsymbol{\Psi}, \tag{15}$$

where

$$\boldsymbol{\Psi}(\boldsymbol{\gamma}^t, \boldsymbol{\omega}^t) = \frac{1}{2} \begin{bmatrix} \boldsymbol{\gamma}^t \\ \boldsymbol{\omega}^t \end{bmatrix}^{\mathrm{T}} \begin{bmatrix} \boldsymbol{C}_T & \mathbf{0}_{3\times 3} \\ \mathbf{0}_{3\times 3} & \boldsymbol{C}_R \end{bmatrix} \begin{bmatrix} \boldsymbol{\gamma}^t \\ \boldsymbol{\omega}^t \end{bmatrix} \tag{16}$$

and extension $\boldsymbol{\gamma}^t$ and shearing $\boldsymbol{\omega}^t$ are the material strain measures

$$\boldsymbol{\gamma}^t = \left(\boldsymbol{R}_t^e\right)^{\mathrm{T}} \left(\partial_s \boldsymbol{\varphi} - \boldsymbol{t}_1\right), \tag{17}$$

and

$$\boldsymbol{C}_T = \mathrm{diag}\left[EA, GA_2, GA_3\right] > 0, \tag{18}$$

$$\boldsymbol{C}_R = \mathrm{diag}\left[GJ, EI_2, EI_3\right] > 0. \tag{19}$$

The constants E and G are interpreted as the Young's modulus and the shear modulus, A is the cross-sectional area of the pipe, A_2 and A_3 are the effective shear areas, $\{I_2, I_3\}$ are the principal moments

of inertia of the cross-section plane relative to principal axes $\boldsymbol{t}_2, \boldsymbol{t}_3$ of $\boldsymbol{\varphi}_r$, and J is the Saint Venant torsional modulus. Hence

$$\boldsymbol{n}^t = \boldsymbol{C}_T \boldsymbol{\gamma}^t \tag{20}$$

$$\boldsymbol{m}^t = \boldsymbol{C}_R \boldsymbol{\omega}^t \tag{21}$$

and in spatial form

$$\boldsymbol{n}^e = \boldsymbol{R}_t^e \boldsymbol{n}^t = \boldsymbol{R}_t^e \boldsymbol{C}_T \left(\boldsymbol{R}_t^e\right)^{\mathrm{T}} \left[\partial_S \boldsymbol{\varphi} - \boldsymbol{t}_1\right], \tag{22}$$

$$\boldsymbol{m}^e = \boldsymbol{R}_t^e \boldsymbol{m}^t = \boldsymbol{R}_t^e \boldsymbol{C}_R \left(\boldsymbol{R}_t^e\right)^{\mathrm{T}} \boldsymbol{\omega}^e. \tag{23}$$

For later use, the time derivative of $\boldsymbol{\gamma}^t$ given in (17) is found to be

$$\dot{\boldsymbol{\gamma}}^t = -\boldsymbol{S}\left(\mathbf{w}^t\right) \left(\boldsymbol{R}_t^e\right)^{\mathrm{T}} \left(\partial_S \boldsymbol{\varphi}\right) + \left(\boldsymbol{R}_t^e\right)^{\mathrm{T}} \left(\partial_S \dot{\boldsymbol{\varphi}}\right) = \left(\boldsymbol{R}_t^e\right)^{\mathrm{T}} \left[\partial_S \dot{\boldsymbol{\varphi}} - \mathbf{w}^e \times \left(\partial_S \boldsymbol{\varphi}\right)\right]. \tag{24}$$

2.5. Dynamics

The equations of motion for the nonlinear pipe model in the spatial frame is

$$m_P \ddot{\boldsymbol{\varphi}} = \partial_S \boldsymbol{n}^e - \boldsymbol{f}_g^e - \boldsymbol{R}_t^e \boldsymbol{f}_D^t \tag{25}$$

$$\boldsymbol{I}_\rho^e \dot{\mathbf{w}}^e + \mathbf{w}^e \times \boldsymbol{I}_\rho^e \mathbf{w}^e = \partial_S \boldsymbol{m}^e + \left(\partial_S \boldsymbol{\varphi}\right) \times \boldsymbol{n}^e - \boldsymbol{D}_R \mathbf{w}^e \tag{26}$$

where

m_P	- mass per unit length
$\boldsymbol{R}_t^e \boldsymbol{f}_D^t$	- transversal hydrodynamic damping matrix
$\boldsymbol{n}^e$	- resultant internal force vector
$\boldsymbol{f}_g^e$	- restoring forces vector (gravitation and buoyancy)
$\boldsymbol{I}_\rho^e$	- mass moment of inertia matrix
$\boldsymbol{D}_R$	- constant damping matrix of rotation
$\boldsymbol{m}^e$	- resultant internal torque vector

The matrix $\boldsymbol{I}_\rho^e\left(S,t\right)$ is the time dependent inertia tensor given by

$$\boldsymbol{I}_\rho^e = \boldsymbol{R}_t^e \boldsymbol{J}_\rho^t \left(\boldsymbol{R}_t^e\right)^{\mathrm{T}}, \quad \boldsymbol{J}_\rho^t = \mathrm{diag}\left[J_1, J_2, J_3\right] \geq \mathbf{0} \tag{27}$$

where $\boldsymbol{J}_\rho^t$ is the inertia tensor for the cross section in the reference configuration.

2.5.1. Hydrostatic Restoring Terms

The pipe is assumed to be completely submerged, and thus the restoring forces per unit length are the sum of the gravitational and the buoyancy, as defined by Archimedes. No moments are generated. The restoring forces acts on the beam in the $\boldsymbol{e}_3$ direction only and is given in $\boldsymbol{e}$ as

$$\boldsymbol{f}_g^e = \left(m_P - \rho_w A\right) g \boldsymbol{e}_3 \tag{28}$$

where ρ_w is the mass density of ambient water and g is the gravitational constant.

2.5.2. Hydrodynamic Damping Terms

The hydrodynamic forces on a submerged body are given by Morison's equation found in (Faltinsen, 1990). For low velocities the added mass term can be neglected. This is a reasonable assumption for risers, mooring lines and pipes. An estimate for the drag forces acting on a cylindrical shape in three dimensions is

$$\boldsymbol{f}_D^t = \frac{1}{2} d \rho_w \boldsymbol{D}_T \begin{bmatrix} \left| v_{r_1}^t \right| v_{r_1}^t \\ \left(\left(v_{r_2}^t \right)^2 + \left(v_{r_3}^t \right)^2 \right)^{1/2} v_{r_2}^t \\ \left(\left(v_{r_2}^t \right)^2 + \left(v_{r_3}^t \right)^2 \right)^{1/2} v_{r_3}^t \end{bmatrix} \tag{29}$$

where d is the outer pipe diameter and

$$\boldsymbol{D}_T = \text{diag}[D_1, D_2, D_3] \geq \boldsymbol{0} \tag{30}$$

where $D_1, D_2, D_3 \geq 0$ are damping coefficients, and the relative velocity $\boldsymbol{v}_r^t$ of the pipe in the water is

$$\boldsymbol{v}_r^t = \left(\boldsymbol{R}_{\boldsymbol{t}}^{\boldsymbol{e}} \right)^{\mathrm{T}} \left(\dot{\boldsymbol{\varphi}}^e - \boldsymbol{v}_c^e \right) \tag{31}$$

where $\boldsymbol{v}_c^e = \boldsymbol{v}_c^e \left(\boldsymbol{\varphi}^{\mathrm{T}} \boldsymbol{e}_3, t \right)$ is the current vector in the inertial frame. The rotational damping is directly proportional to the angular velocity, and

$$\boldsymbol{D}_R = \text{diag}[D_4, D_5, D_6] \geq \boldsymbol{0} \tag{32}$$

where $D_4, D_5, D_6 \geq 0$ are damping coefficients.

2.6. Boundary Conditions

2.6.1. Seabed

The lower end of the pipe is assumed to be fixed to the seabed. The boundary condition for $S = 0$ is thus

$$\boldsymbol{\varphi}(0,t) = \boldsymbol{\varphi}_0 = 0, \quad \boldsymbol{R}_t^e(0,t) = \boldsymbol{R}_{t,0}^e = \boldsymbol{I}_{3\times 3} \tag{33}$$

2.6.2. Vessel

The upper end of the pipe is fixed to a surface vessel, which will be the boundary condition at $S = L$. In recent years there has been a significant drive to develop time-domain models for simulation and control system design based on data obtained from seakeeping programs such as ShipX and WAMIT. These programs use potential theory to compute the potential coefficients (added mass and potential damping) and the existing wave loads (Froude-Krylov and diffraction forces) for a given vessel design (Fossen, 2002) and (Fossen and Smogeli, 2004). Following Perez and Fossen (2007), a potential theory formulation for a surface vessel suited for dynamic positioning and low speed manoeuvring is developed. This model is adopted as the boundary condition of the pipe at $S = L$, $\boldsymbol{\varphi}(L,t)$ and $\boldsymbol{R}_t^e(L,t) = \boldsymbol{R}_b^e(t)(R_b^t)^{\mathrm{T}}$.

Let $\boldsymbol{\eta} \in \mathbb{R}^3 \times \mathcal{S}^3$ be the generalized coordinate position vector given in the spatial frame $\boldsymbol{e}$ and $\boldsymbol{\nu} \in \mathbb{R}^6$ be the generalized velocity vector given in the body frame $\boldsymbol{b}$, both defined by Fossen (2002) as

$$\boldsymbol{\eta} = [x, y, z, \phi, \theta, \psi]^{\mathrm{T}} \qquad \text{and} \qquad \boldsymbol{\nu} = [u, v, w, p, q, r]^{\mathrm{T}} \tag{34}$$

Note that Euler angles are used to represent the vessel attitude. The equations of motion are linear and given by

$$\dot{\boldsymbol{\eta}} = \boldsymbol{J}(\boldsymbol{\eta})\boldsymbol{\nu} \tag{35}$$

$$\boldsymbol{M}\dot{\boldsymbol{\nu}} + \boldsymbol{C}_{RB}\boldsymbol{\nu} + \boldsymbol{C}_A\boldsymbol{\nu} + \boldsymbol{B}(\infty)\boldsymbol{\nu} + \boldsymbol{\mu} + \boldsymbol{G}\boldsymbol{\eta} = \boldsymbol{\tau}^b + \bar{\boldsymbol{\tau}}^b. \tag{36}$$

Let

$$\boldsymbol{M} \triangleq \boldsymbol{M}_{RB} + \boldsymbol{M}_A \tag{37}$$

where the rigid body inertia matrix $\boldsymbol{M}_{RB}$ is found from Euler's first and second axioms of conservation of linear and angular momentum and is given by

$$\boldsymbol{M}_{RB} = \begin{bmatrix} m_V \boldsymbol{I}_{3\times 3} & \boldsymbol{0}_{3\times 3} \\ \boldsymbol{0}_{3\times 3} & \boldsymbol{I}_V^b \end{bmatrix} \tag{38}$$

where m_V is the total vessel mass and $\boldsymbol{I}_V^b = \mathrm{diag}[I_a, I_b, I_c] \in \mathbb{R}^{3\times 3}$ is the body inertia tensor. $\boldsymbol{M}_A = \boldsymbol{A}(\infty)$ and $\boldsymbol{B}(\infty)$ are the constant infinite frequency added mass and potential damping matrices. As the frame used is not inertial, the Coriolis and centripetal terms for the rigid body $\boldsymbol{C}_{RB}$ and the added mass $\boldsymbol{C}_A$ are accounted for and appears as

$$\boldsymbol{C}_{RB} \triangleq \boldsymbol{M}_{RB} U \boldsymbol{L} \quad \text{and} \quad \boldsymbol{C}_A \triangleq \boldsymbol{M}_A U \boldsymbol{L} \tag{39}$$

where $U = \|\boldsymbol{v}^e\|$, and

$$\boldsymbol{L} \triangleq \begin{bmatrix} 0 & \cdots & 0 & 0 \\ 0 & \cdots & 0 & 1 \\ 0 & \cdots & -1 & 0 \\ \vdots & \ddots & \vdots & \vdots \\ 0 & \cdots & 0 & 0 \end{bmatrix} \in \mathbb{R}^{6\times 6}. \tag{40}$$

The matrix $\boldsymbol{G}$ is the restoring matrix. From the computation of the radiation forces the term

$$\bar{\boldsymbol{\tau}}^b \triangleq \boldsymbol{B}(\infty)\bar{\boldsymbol{\nu}} \tag{41}$$

appears where $\bar{\boldsymbol{\nu}}$ is the requested velocity in the body frame, equivalent to $\boldsymbol{v}^e$ in the inertial frame. External forces including control forces are collected in the $\boldsymbol{\tau}^b$ vector.

For t the term $\boldsymbol{\mu}$ is a convolution term representing the fluid memory effects and given as

$$\boldsymbol{\mu} \triangleq \int_0^t \boldsymbol{K}(t-\xi)\left[\boldsymbol{\nu}(\xi) + U\boldsymbol{L}\boldsymbol{\eta}(\xi)\right] d\xi \tag{42}$$

where $\boldsymbol{K}(t)$ is a matrix of retardation functions (Ogilvie, 1964):

$$\boldsymbol{K}(t) = \int_0^\infty (\boldsymbol{B}(\omega) - \boldsymbol{B}(\infty))\cos(\omega t)\, d\omega. \tag{43}$$

For the pipeline installation application, and following Kristiansen et al. (2005), $U \approx 0$. Hence $\boldsymbol{B}(\infty) = 0$ and (42) reduces to

$$\boldsymbol{\mu}(t) \triangleq \int_0^t \boldsymbol{K}(t-\xi)\boldsymbol{\nu}(\xi)\, d\xi \tag{44}$$

$$= \boldsymbol{H}(s)\boldsymbol{\nu} \tag{45}$$

$$\approx \boldsymbol{D}_p\boldsymbol{\nu} \tag{46}$$

where $\boldsymbol{D}_p = \boldsymbol{H}(0)$ is a frequency-independent constant matrix approximating the transfer matrix $\boldsymbol{H}(s)$ at low frequencies. Further more $\bar{\boldsymbol{\tau}}^b = \mathbf{0}$ and the resulting linear state-space model becomes

$$\boldsymbol{M}\dot{\boldsymbol{\nu}} + \boldsymbol{C}_{RB}\boldsymbol{\nu} + \boldsymbol{C}_A\boldsymbol{\nu} + \boldsymbol{D}_p\boldsymbol{\nu} + \boldsymbol{G}\boldsymbol{\eta} = \boldsymbol{\tau}^b. \tag{47}$$

In hydrodynamics it is common to assume linear super position (Faltinsen, 1990). Nonlinear Coriolis and damping terms can be added directly in the time-domain model (47) according to:

$$\boldsymbol{M}\dot{\boldsymbol{\nu}} + \boldsymbol{C}(\boldsymbol{\nu})\boldsymbol{\nu} + \boldsymbol{D}(\boldsymbol{\nu})\boldsymbol{\nu} + \boldsymbol{g}(\boldsymbol{\varphi}, \boldsymbol{R}_b^e) = \boldsymbol{\tau}^b \tag{48}$$

with relaxations

$$\boldsymbol{G}\boldsymbol{\eta} \longleftrightarrow \boldsymbol{g}(\boldsymbol{\varphi}, \boldsymbol{R}_b^e) \tag{49}$$

$$\boldsymbol{C}_{RB} \longleftrightarrow \boldsymbol{C}_{RB}(\boldsymbol{\nu}) \tag{50}$$

$$\boldsymbol{C}_A \longleftrightarrow \boldsymbol{C}_A(\boldsymbol{\nu}) \tag{51}$$

and

$$\boldsymbol{C}(\boldsymbol{\nu}) = \boldsymbol{C}_{RB}(\boldsymbol{\nu}) + \boldsymbol{C}_A(\boldsymbol{\nu}) \tag{52}$$

$$\boldsymbol{D}(\boldsymbol{\nu}) = \boldsymbol{D}_p + \boldsymbol{D}_v(\boldsymbol{\nu}) \tag{53}$$

where $\boldsymbol{D}_v(\boldsymbol{\nu})$ is quadratic viscous damping due to cross-flow drag and surge resistance. Note that $\boldsymbol{\tau}^b = \boldsymbol{\tau}_{ctrl}^b + \boldsymbol{\tau}_{exc}^b$ if control forces are applied to the vessel.

A metacentric stable surface vessel has restoring forces and moments in heave, roll ϕ and pitch θ that will resist inclinations away from the steady-state equilibrium. The restoring forces and moments will depend on the vessel's metacentric height, the location of the center of gravity (CG), the center of buoyancy (CB) and the shape and size of the water plane, denoted by A_{wp}. For every vessel and load a transversal metacentric height $\overline{GM}_T \in \mathbb{R}$ and a longitudinal metacentric height $\overline{GM}_L \in \mathbb{R}$ can be computed.

The equilibrium in heave is obtained when the gravity and buoyancy forces balance. When the heave position $\boldsymbol{\varphi}^{\mathrm{T}}(L,t)\,\boldsymbol{e}_3$ is changed due to external forces, or the heave equilibrium z_{eq} change due to i.e. waves, a force $\boldsymbol{g}_l^e \in \mathbb{R}^3$ is generated to restore the balance. This force is modeled in the $\boldsymbol{e}$ frame by

$$\boldsymbol{g}_l^e = -A_{wp}\rho_w g\left(\boldsymbol{\varphi}^{\mathrm{T}}(L,t)\,\boldsymbol{e}_3 - z_{eq}\right)\boldsymbol{e}_3 \tag{54}$$

where A_{wp} is assumed to be constant for small changes in heave.

From geometric considerations, the moment arms in roll and pitch can be found to be

$$\boldsymbol{r}_r^b = \begin{bmatrix} -\overline{GM}_L \sin\theta \\ \overline{GM}_T \sin\phi \\ 0 \end{bmatrix}. \tag{55}$$

The pipe model is developed without Euler angles and it is thus desired to avoid these in the vessel mode. The Euler angles are removed from the equation by observing that

$$\sin\theta = -\left(\boldsymbol{R}_b^e\boldsymbol{e}_1\right)^{\mathrm{T}}\boldsymbol{e}_3 \tag{56}$$

$$\sin\phi \approx \cos\theta\sin\phi = \left(\boldsymbol{R}_b^e\boldsymbol{e}_2\right)^{\mathrm{T}}\boldsymbol{e}_3 \tag{57}$$

The approximation $\cos\theta = 1$ is generally true for small pitch angles. Equation (55) now becomes

$$\boldsymbol{r}_r^b = \begin{bmatrix} \overline{GM}_L \left(\boldsymbol{R}_b^e \boldsymbol{e}_1\right)^{\mathrm{T}} \boldsymbol{e}_3 \\ \overline{GM}_T \left(\boldsymbol{R}_b^e \boldsymbol{e}_2\right)^{\mathrm{T}} \boldsymbol{e}_3 \\ 0 \end{bmatrix} \tag{58}$$

and the restoring moment term is thus

$$\begin{aligned} \boldsymbol{g}_r^e &= \boldsymbol{r}_r^e \times \boldsymbol{f}_r^e \\ &= \left(\boldsymbol{R}_b^e \boldsymbol{r}_r^b\right) \times \left(m_V g \boldsymbol{e}_3\right). \end{aligned} \tag{59}$$

It is assumed that there is no moment due to heave. Thus the nonlinear restoring forces term of (48) is given in the body frame $\boldsymbol{b}$ as

$$\boldsymbol{g}^b\left(\boldsymbol{\varphi}\left(L,t\right), \boldsymbol{R}_b^e\left(t\right)\right) = \begin{bmatrix} \left(\boldsymbol{R}_b^e\right)^{\mathrm{T}} \boldsymbol{g}_t^e \\ \left(\boldsymbol{R}_b^e\right)^{\mathrm{T}} \boldsymbol{g}_r^e \end{bmatrix}. \tag{60}$$

The spatial representation of (48) is obtained by applying the following kinematic transformations:

$$\begin{aligned} \boldsymbol{\eta} &= \boldsymbol{J}\boldsymbol{\nu} \qquad &\Leftrightarrow \qquad \boldsymbol{\nu} &= \boldsymbol{J}^{-1}\boldsymbol{\eta} \\ \dot{\boldsymbol{\eta}} &= \dot{\boldsymbol{J}}\boldsymbol{\nu} + \boldsymbol{J}\dot{\boldsymbol{\nu}} \qquad &\Leftrightarrow \qquad \dot{\boldsymbol{\nu}} &= \boldsymbol{J}^{-1}\left(\dot{\boldsymbol{\eta}} - \dot{\boldsymbol{J}}\boldsymbol{J}^{-1}\boldsymbol{\eta}\right) \end{aligned} \tag{61}$$

where

$$\boldsymbol{J} = \begin{bmatrix} \boldsymbol{R}_b^e & \boldsymbol{0}_{3\times 3} \\ \boldsymbol{0}_{3\times 3} & \boldsymbol{R}_b^e \end{bmatrix} \in \mathbb{R}^{6\times 6} \quad \text{and} \quad \boldsymbol{J}^{-1} = \boldsymbol{J}^{\mathrm{T}}. \tag{62}$$

The resulting spatial vector representation of (48) is

$$\boldsymbol{M}_\eta(\boldsymbol{\eta})\ddot{\boldsymbol{\eta}} + \boldsymbol{C}_\eta(\boldsymbol{\eta},\dot{\boldsymbol{\eta}})\dot{\boldsymbol{\eta}} + \boldsymbol{D}_\eta(\boldsymbol{\eta},\dot{\boldsymbol{\eta}})\dot{\boldsymbol{\eta}} + \boldsymbol{g}_\eta(\boldsymbol{\varphi},\boldsymbol{R}_b^e) = \boldsymbol{J}\boldsymbol{\tau}^b \tag{63}$$

where

$$\boldsymbol{M}_\eta\left(\boldsymbol{\eta}\right) = \boldsymbol{J}\boldsymbol{M}\boldsymbol{J}^{-1} \tag{64}$$

$$\boldsymbol{C}_\eta\left(\boldsymbol{\eta},\dot{\boldsymbol{\eta}}\right) = \boldsymbol{J}\left[\boldsymbol{C}\left(\boldsymbol{\eta}\right) - \boldsymbol{M}\boldsymbol{J}^{-1}\dot{\boldsymbol{J}}\right]\boldsymbol{J}^{-1} \tag{65}$$

$$\boldsymbol{D}_\eta\left(\boldsymbol{\eta},\dot{\boldsymbol{\eta}}\right) = \boldsymbol{J}\boldsymbol{D}\left(\boldsymbol{\eta}\right)\boldsymbol{J}^{-1} \tag{66}$$

$$\boldsymbol{g}_\eta\left(\boldsymbol{\varphi},\boldsymbol{R}_b^e\right) = \boldsymbol{J}\boldsymbol{g}\left(\boldsymbol{\varphi},\boldsymbol{R}_b^e\right) \tag{67}$$

The following properties of (63) holds as $\boldsymbol{M} = \boldsymbol{M}^{\mathrm{T}} > \boldsymbol{0}$ and $\dot{\boldsymbol{M}} = \boldsymbol{0}$:

P1) $\boldsymbol{M}_\eta\left(\boldsymbol{\eta}\right) = \boldsymbol{M}_\eta^{\mathrm{T}}\left(\boldsymbol{\eta}\right) > 0, \quad \forall\ \boldsymbol{\eta} \in \mathbb{R}^6$

P2) $\boldsymbol{s}^{\mathrm{T}}\left[\dot{\boldsymbol{M}}_\eta\left(\boldsymbol{\eta}\right) - 2\boldsymbol{C}_\eta\left(\boldsymbol{\eta},\dot{\boldsymbol{\eta}}\right)\right]\boldsymbol{s} = 0, \quad \forall\ \boldsymbol{s},\boldsymbol{\eta} \in \mathbb{R}^6$

P3) $\boldsymbol{D}_\eta\left(\boldsymbol{\eta},\dot{\boldsymbol{\eta}}\right) > 0, \quad \forall\ \boldsymbol{\eta} \in \mathbb{R}^6$

Note that the skew-symmetry property of $\boldsymbol{C}$ does not hold for $\boldsymbol{C}_\eta$. These properties will be used in the later passivity analysis. When transforming from a moving frame to an inertial frame the Coriolis terms of the linear motion are canceled.

Let the pipe be fixed to the center of gravity of the vessel such that

$$\dot{\boldsymbol{\eta}} = \begin{bmatrix} \dot{\boldsymbol{\varphi}}(L,t) \\ \mathbf{w}^e(L,t) \end{bmatrix} \quad \text{and} \quad \ddot{\boldsymbol{\eta}} = \begin{bmatrix} \ddot{\boldsymbol{\varphi}}(L,t) \\ \dot{\mathbf{w}}^e(L,t) \end{bmatrix}. \tag{68}$$

The forces and moments acting between the pipe and vessel are for the total system internal forces, and by Newton's third law the following relationship holds:

$$\boldsymbol{J}\boldsymbol{\tau}^b = -\begin{bmatrix} \boldsymbol{n}^e(L,t) \\ \boldsymbol{m}^e(L,t) \end{bmatrix}. \tag{69}$$

3. Passivity

In this section the system is shown to be input-output passive based on the energy functions of the pipe and the vessel respectively. Let the total energy of the system be given as

$$\mathcal{E} = \mathcal{E}_P + \mathcal{E}_V \geq 0 \tag{70}$$

where $\mathcal{E}_P$ and $\mathcal{E}_V$ are respectively the total energy of the pipe and the surface vessel. The pipe energy function, $\mathcal{E}_P$ is the sum of kinetic energy $\mathcal{T}_P$ and potential energy $\mathcal{U}_P$ (Simo and Vu-Quoc, 1986),

$$\mathcal{E}_P = \mathcal{T}_P + \mathcal{U}_P \tag{71}$$

where

$$\mathcal{T}_P = \frac{1}{2}\int_0^L m_p \left\|\dot{\boldsymbol{\varphi}}\right\|_2^2 + \left\langle \mathbf{w}^e, \boldsymbol{I}_\rho^e \mathbf{w}^e \right\rangle dS \tag{72}$$

$$\mathcal{U}_P = \int_0^L \boldsymbol{\Psi}\left(\boldsymbol{\gamma}^t, \boldsymbol{\omega}^t\right) dS + \int_0^L \left\langle \boldsymbol{f}_g^e, \boldsymbol{\varphi} \right\rangle dS. \tag{73}$$

The vessel energy function $\mathcal{E}_V$ is the sum of the kinetic $\mathcal{T}_V$ and potential energy $\mathcal{U}_V$,

$$\mathcal{E}_V = \mathcal{T}_V + \mathcal{U}_V \tag{74}$$

where

$$\mathcal{T}_V = \frac{1}{2}\boldsymbol{\nu}^{\mathrm{T}}\boldsymbol{M}\boldsymbol{\nu}. \tag{75}$$

and

$$\begin{aligned} \mathcal{U}_V =& \frac{1}{2}A_{wp}\rho_w g\left(\boldsymbol{\varphi}^{\mathrm{T}}(L,t)\, e_3 + h_{ref}\right)^2 + \\ & \frac{1}{2}m_V g\left\{GM_L\left[\left(\boldsymbol{R}_b^e \boldsymbol{e}_1\right)^{\mathrm{T}} \boldsymbol{e}_3\right]^2 + GM_T\left[\left(\boldsymbol{R}_b^e \boldsymbol{e}_2\right)^{\mathrm{T}} \boldsymbol{e}_3\right]^2\right\} \end{aligned} \tag{76}$$

Equations (75) and (76) are given in $\boldsymbol{b}$. The time derivative of (70) is given as:

$$\dot{\mathcal{E}} = \dot{\mathcal{E}}_P + \dot{\mathcal{E}}_V. \tag{77}$$

For the pipe $\dot{\mathcal{E}}_P$ is given as the sum of the derivatives of the kinetic energy $\dot{\mathcal{T}}_P$ and potential energy $\dot{\mathcal{U}}_P$ respectively, where

$$\dot{\mathcal{T}}_P = \int_0^L \langle \dot{\boldsymbol{\varphi}}, m_p \ddot{\boldsymbol{\varphi}} \rangle + \left\langle \mathbf{w}^e, \boldsymbol{I}_\rho^e \dot{\mathbf{w}}^e \right\rangle \, dS = \int_0^L \left\langle \dot{\boldsymbol{\varphi}}, \left[\partial_S \boldsymbol{n}^e - \boldsymbol{f}_g^e - \boldsymbol{R}_t^e \boldsymbol{f}_D^t \right] \right\rangle \, dS + \int_0^L \left\langle \mathbf{w}^e, \left[(\boldsymbol{I}_\rho^e \mathbf{w}^e \times \mathbf{w}^e) + \partial_S \boldsymbol{m}^e + (\partial_S \boldsymbol{\varphi}) \times \boldsymbol{n}^e - \boldsymbol{D}_R \mathbf{w}^e \right] \right\rangle \, dS \tag{78}$$

and

$$\begin{aligned} \dot{\mathcal{U}}_P &= \int_0^L \left\langle \boldsymbol{n}^t, \dot{\boldsymbol{\gamma}}^t \right\rangle + \left\langle \boldsymbol{m}^t, \dot{\boldsymbol{\omega}}^t \right\rangle \, dS + \int_0^L \left\langle \boldsymbol{f}_g^e, \dot{\boldsymbol{\varphi}} \right\rangle \, dS \\ &= \int_0^L \langle \boldsymbol{n}^e, [\partial_S \dot{\boldsymbol{\varphi}} - (\mathbf{w}^e \times (\partial_S \boldsymbol{\varphi}))] \rangle \, dS + \int_0^L \langle \boldsymbol{m}^e, [\partial_S \mathbf{w}^e + (\boldsymbol{\omega}^e \times \mathbf{w}^e)] \rangle \, dS + \int_0^L \left\langle \boldsymbol{f}_g^e, \dot{\boldsymbol{\varphi}} \right\rangle \, dS \\ &= \langle \boldsymbol{n}^e, \dot{\boldsymbol{\varphi}} \rangle \Big|_0^L + \langle \boldsymbol{m}^e, \mathbf{w}^e \rangle \Big|_0^L - \int_0^L \langle \partial_S \boldsymbol{n}^e, \dot{\boldsymbol{\varphi}} \rangle + \langle \partial_S \boldsymbol{m}^e, \mathbf{w}^e \rangle + \langle \mathbf{w}^e, (\partial_S \boldsymbol{\varphi}) \times \boldsymbol{n}^e \rangle \, dS + \int_0^L \left\langle \boldsymbol{f}_g^e, \dot{\boldsymbol{\varphi}} \right\rangle \, dS \end{aligned} \tag{79}$$

$$\dot{\mathcal{E}}_P = \langle \boldsymbol{n}^e, \dot{\boldsymbol{\varphi}} \rangle \Big|_0^L + \langle \boldsymbol{m}^e, \mathbf{w}^e \rangle \Big|_0^L - \int_0^L \left\langle \dot{\boldsymbol{\varphi}}, \boldsymbol{R}_t^e \boldsymbol{f}_D^t \right\rangle dS - \int_0^L \langle \mathbf{w}^e, \boldsymbol{D}_R \mathbf{w}^e \rangle \, dS \tag{80}$$

If the terms related to damping in equation (80) are neglected, only the boundary conditions are effecting the energy, and the pipe is seen to be energy conservative. Investigating the integral term for the rotational damping it is readily seen that

$$\int_0^L \langle \mathbf{w}^e, \boldsymbol{D}_R \mathbf{w}^e \rangle \, dS = \int_0^L \left(\sum_{i=1}^3 D_{i+3} \left(\mathbf{w}_i^e \right)^2 \right) dS \geq 0 \quad \forall \mathbf{w}^e \tag{81}$$

such that this term will always have a negative contribution. The restoring term is rewritten into

$$\int_0^L \left\langle \dot{\boldsymbol{\varphi}}, \boldsymbol{R}_t^e \boldsymbol{f}_D^t \right\rangle dS = \frac{1}{2} d \rho_w \int_0^L \langle \dot{\boldsymbol{\varphi}}, \boldsymbol{\Pi} (\dot{\boldsymbol{\varphi}} - \boldsymbol{v}_c^e) \rangle \, dS \geq 0, \quad \forall \ \left| v_{c,i}^e \right| \leq |\dot{\varphi}_i| \tag{82}$$

where

$$\boldsymbol{\Pi} = \boldsymbol{R}_t^e \boldsymbol{D}_T \boldsymbol{\Gamma} \left(\boldsymbol{R}_t^e \right)^{\mathrm{T}} \geq \mathbf{0}, \tag{83}$$

$$\boldsymbol{\Gamma} = \operatorname{diag} \left[\left| v_{r_1}^t \right|, \left(\left(v_{r_2}^t \right)^2 + \left(v_{r_3}^t \right)^2 \right)^{1/2}, \left(\left(v_{r_2}^t \right)^2 + \left(v_{r_3}^t \right)^2 \right)^{1/2} \right] \geq \mathbf{0}. \tag{84}$$

The current in the water is an external force which is present in this equation. In order to establish stability of the pipe, assume no current such that $\boldsymbol{v}_c^e = \mathbf{0}$. Then it is evident that $\dot{\mathcal{E}}_P \leq \mathbf{0}$ which proves that the pipe model is asymptotically stable. Note that this property will hold as long as $|(v_c^e)_i| < |\dot{\varphi}_i|$.

Considering the vessel, equations (75) and (76) are differentiated to find $\dot{\mathcal{T}}_V$ and $\dot{\mathcal{U}}_V$. Applying equation (48) and property **P2** in the appropriate reference frame to the resulting equations,

$$\dot{\mathcal{T}}_V = \boldsymbol{\nu}^{\mathrm{T}} \boldsymbol{\tau}^b - \boldsymbol{\nu} \mathrm{T} - \boldsymbol{D} \boldsymbol{\nu} - \boldsymbol{\nu}^{\mathrm{T}} \boldsymbol{g}^b \tag{85}$$

$$\dot{\mathcal{U}}_V = \boldsymbol{\nu}^{\mathrm{T}} \boldsymbol{g}^b. \tag{86}$$

Summing equations (85) and (86) yields $\dot{\mathcal{E}}$ as

$$\dot{\mathcal{E}}_V = \boldsymbol{\nu}^{\mathrm{T}}\boldsymbol{\tau}^b - \boldsymbol{\nu}^{\mathrm{T}}\boldsymbol{D}\boldsymbol{\nu}. \tag{87}$$

Applying property **P3**, to equation (87) yields $\dot{\mathcal{E}}_V \leq \boldsymbol{\nu}^{\mathrm{T}}\boldsymbol{\tau}^b$, which shows that the vessel is input-output passive with input $\boldsymbol{\tau}$ and output $\boldsymbol{\nu}$.

The derivative of the energy of the total system in equation (77) can now be found from equations (80) and (87). The lower boundary condition $S = 0$ is given as

$$\langle \boldsymbol{n}^e, \dot{\boldsymbol{\varphi}} \rangle \,|_0 = \langle \boldsymbol{m}^e, \mathbf{w}^e \rangle \,|_0 = 0, \tag{88}$$

and the upper boundary condition is given by equation (69) where the pipe is connected to the vessel in the center of gravity, as defined in equation (68). The total rate of change of energy of the pipe and vessel system is

$$\begin{aligned}
\dot{\mathcal{E}} =& \langle \boldsymbol{n}^e, \dot{\boldsymbol{\varphi}} \rangle \,|_0^L + \langle \boldsymbol{m}^e, \mathbf{w}^e \rangle \,|_0^L - \int_0^L \left\langle \dot{\boldsymbol{\varphi}}, \boldsymbol{R}_t^e \boldsymbol{f}_D^t \right\rangle dS \\
&- \int_0^L \langle \mathbf{w}^e, \boldsymbol{D}_R \mathbf{w}^e \rangle \, dS + \boldsymbol{\eta}^{\mathrm{T}}\boldsymbol{\tau}^e - \boldsymbol{\eta}^{\mathrm{T}}\boldsymbol{D}_\eta\boldsymbol{\eta} \\
=& - \int_0^L \left\langle \dot{\boldsymbol{\varphi}}, \boldsymbol{R}_t^e \boldsymbol{f}_D^t \right\rangle dS - \int_0^L \langle \mathbf{w}^e, \boldsymbol{D}_R \mathbf{w}^e \rangle \, dS - \boldsymbol{\eta}^{\mathrm{T}}\boldsymbol{D}_\eta\boldsymbol{\eta} \\
\leq& 0
\end{aligned} \tag{89}$$

which implies that the system dissipates energy. By considering the energy function as a cost function, Lyapunov analysis shows that the combined system is asymptotically stable. If a control force $\boldsymbol{\tau}_{control}$ is added in the vessel model (48), the analysis will show that the system is input-output passive with the control force $\boldsymbol{\tau}_{control}$ as the input and the vessel velocity $\boldsymbol{\nu}$ as the output, that is

$$\dot{\mathcal{E}} \leq \boldsymbol{\nu}^{\mathrm{T}}\boldsymbol{\tau}_{control}^b. \tag{90}$$

4. Application Example

The case of offshore pipeline installation is investigated in this section. Pipelines are installed with purpose build pipelay vessels with dynamic positioning systems. The pipe is clamped on to the vessel by heavy tension equipment, and is extended by pipe elements welded onto the pipe end in a production line accommodating either S-lay or J-lay, which are the two main pipelay methods. The two methods are seen to be complementary in Parinet and Frazer (2007). The methods are well described in recent text books on pipelaying, such as Braestrup et al. (2005), Guo et al. (2005) and Palmer and King (2004). The present trends in deepwater pipelay systems in general are well described by Heerema (2005) and the references therein. The coefficient matrices for the vessel is obtained from the Marine Systems Simulator (MSS) available at (Fossen and Perez, 2004).

4.1. Numerical Implementation

A FEM is implemented for numerical simulations. Taking the inner product of (25)–(26) with admissible test functions

$$\mathcal{V} = \{(\boldsymbol{u}, \boldsymbol{\vartheta}) \,|\, S \in [0, L] \to \mathbb{R}^3 \times \mathbb{R}^3 \,|\, (\boldsymbol{u}, \boldsymbol{\vartheta})\big|_{S=0} = (\boldsymbol{0}, \boldsymbol{0})\}, \tag{91}$$

such that

$$T_{(\boldsymbol{\varphi}, \boldsymbol{R}_t^e)}\mathcal{C} := \{(\boldsymbol{u}, \boldsymbol{S}(\boldsymbol{\vartheta})\boldsymbol{R}_t^e) \,|\, (\boldsymbol{u}, \boldsymbol{\vartheta}) \in \mathcal{V}\}, \tag{92}$$

to obtain (using Gauss's theorem) the weak formulation of the initial boundary problem (25)–(26), with boundary conditions (33) and (69),

$$\begin{aligned} G_{\text{dyn}}(\boldsymbol{\Phi}, \boldsymbol{R}_t^e; \boldsymbol{u}, \boldsymbol{\vartheta}) \triangleq & \int_0^L \langle m_P(\ddot{\boldsymbol{\varphi}}), \boldsymbol{u}\rangle + \langle [\boldsymbol{I}_\rho(\dot{\mathbf{w}}^e) + \mathbf{w}^e \times (\boldsymbol{I}_\rho \mathbf{w}^e)], \boldsymbol{\vartheta}\rangle \, dS + \\ & \int_0^L \langle \boldsymbol{f}_g^e, \boldsymbol{u}\rangle + \langle \boldsymbol{D}_R \mathbf{w}^e, \boldsymbol{\vartheta}\rangle \, dS + G_{\text{stat}}(\boldsymbol{\Phi}, \boldsymbol{R}_t^e; \boldsymbol{u}, \boldsymbol{\vartheta}) + \\ & \left\langle [\boldsymbol{M}_\eta(\boldsymbol{\eta})\ddot{\boldsymbol{\eta}} + \boldsymbol{C}_\eta(\boldsymbol{\eta}, \dot{\boldsymbol{\eta}})\dot{\boldsymbol{\eta}} + \boldsymbol{D}_\eta(\boldsymbol{\eta}, \dot{\boldsymbol{\eta}})\dot{\boldsymbol{\eta}}], (\boldsymbol{u}^{\mathrm{T}}, \boldsymbol{\vartheta}^{\mathrm{T}})^{\mathrm{T}} \right\rangle \Big|_{S=L} = 0, \end{aligned} \tag{93}$$

for all test functions $(\boldsymbol{u}, \boldsymbol{\vartheta}) \in \mathcal{V}$, where (the static part)

$$\begin{aligned} G_{\text{stat}}(\boldsymbol{\Phi}, \boldsymbol{R}_t^e; \boldsymbol{u}, \boldsymbol{\vartheta}) \triangleq & \int_0^L \left\langle \boldsymbol{n}^e, \left[\frac{d\boldsymbol{u}}{dS} - \boldsymbol{S}(\boldsymbol{\vartheta})(\partial_S \boldsymbol{\varphi})\right] \right\rangle + \left\langle \boldsymbol{m}^e, \frac{d\boldsymbol{\vartheta}}{dS} \right\rangle dS + \\ & \int_0^L \langle \boldsymbol{f}_g^e, \boldsymbol{u}\rangle \, dS + \left\langle \boldsymbol{g}_\eta(\boldsymbol{\varphi}, \boldsymbol{R}_b^e), (\boldsymbol{u}^{\mathrm{T}}, \boldsymbol{\vartheta}^{\mathrm{T}})^{\mathrm{T}} \right\rangle \Big|_{S=L}. \end{aligned} \tag{94}$$

Parameterizing of the rotation matrix $\boldsymbol{R}_t^e$ in Euler angles $\boldsymbol{\Theta} = (\phi, \theta, \psi)^{\mathrm{T}} \to \boldsymbol{R}_t^e(\boldsymbol{\Theta})$, locally diffeomorphic to $SO(3) \simeq \mathbb{RP}^3$, yields the transformations

$$\begin{aligned} \mathbf{w}^e &= \boldsymbol{\Pi}_e \dot{\boldsymbol{\Theta}}, & \dot{\mathbf{w}}^e &= \boldsymbol{\Pi}_e \ddot{\boldsymbol{\Theta}} + \dot{\boldsymbol{\Pi}}_e \dot{\boldsymbol{\Theta}}, \\ \partial_S \boldsymbol{\omega}^e &= \boldsymbol{\Pi}_e (\partial_S \boldsymbol{\Theta}), & \boldsymbol{\Theta} &= (\phi, \theta, \psi)^{\mathrm{T}}, \end{aligned} \tag{95}$$

where

$$\boldsymbol{\Pi}_e = \begin{bmatrix} \cos\theta\cos\psi & -\sin\psi & 0 \\ \cos\theta\sin\psi & \cos\psi & 0 \\ -\sin\theta & 0 & 1 \end{bmatrix}. \tag{96}$$

Hence, the configuration space for Euler angles becomes

$$\widetilde{\mathcal{C}} := \{(\boldsymbol{\varphi}, \boldsymbol{\Theta}) | S \in [0, L] \to \mathbb{R}^3 \times \mathbb{R}^3 \,|\, \langle \partial_S \boldsymbol{\varphi}(S), \boldsymbol{R}_t^e(\boldsymbol{\Theta})\rangle \boldsymbol{e}_1 > 0\} \tag{97}$$

with test functions

$$\widetilde{\mathcal{V}} := \{(\boldsymbol{u}, \widetilde{\boldsymbol{\vartheta}}) \,|\, S \in [0, L] \to \mathbb{R}^3 \times \mathbb{R}^3 \,|\, (\boldsymbol{u}, \widetilde{\boldsymbol{\vartheta}})\big|_{S=0} = (\boldsymbol{0}, \boldsymbol{0})\}, \tag{98}$$

such that

$$T_{(\boldsymbol{\varphi}, \boldsymbol{\Theta})}\widetilde{\mathcal{C}} := \{(\boldsymbol{u}, \widetilde{\boldsymbol{\vartheta}}) \,|\, (\boldsymbol{u}, \widetilde{\boldsymbol{\vartheta}}) \in \widetilde{\mathcal{V}}\}. \tag{99}$$

The weak formulation (93) for the configuration space (97) is semi discretized in N nodes with uniform sub interval $\bigcup_{i=1}^{N-1}[S_i, S_{i+1}] = [0, L]$, and using linear shape functions $N_h^i(S)$ such that

$$\begin{aligned} \boldsymbol{\varphi} \approx \boldsymbol{\varphi}_h &= \textstyle\sum_{i=1}^N \boldsymbol{\varphi}_i(t) N_h^i(S), & \boldsymbol{\Theta} \approx \boldsymbol{\Theta}_h &= \textstyle\sum_{i=1}^N \boldsymbol{\Theta}_i(t) N_h^i(S), \\ \boldsymbol{u}_h &= \textstyle\sum_{i=1}^N \boldsymbol{u}_i N_h^i(S), & \widetilde{\boldsymbol{\vartheta}}_h &= \textstyle\sum_{i=1}^N \widetilde{\boldsymbol{\vartheta}}_i N_h^i(S), \end{aligned} \tag{100}$$

The semi discretized problem is finally obtained on the form

$$\widetilde{\boldsymbol{M}}_h(\boldsymbol{x}_i)\dot{\boldsymbol{x}}_i = \widetilde{\boldsymbol{F}}_h(\boldsymbol{x}_i), \qquad \boldsymbol{x}(t) \in \mathbb{R}^{12N} \tag{101}$$

where

$$\boldsymbol{x}_i = \left[\boldsymbol{\varphi}_i, \boldsymbol{\Theta}_i, \dot{\boldsymbol{\varphi}}_i, \dot{\boldsymbol{\Theta}}_i\right]^{\mathrm{T}}, \quad \text{for } i = 1, \ldots, N, \tag{102}$$

$\widetilde{\boldsymbol{M}}_h(\boldsymbol{x}_i) \in \mathbb{R}^{12N\times 12N}$ is the system mass matrix, and $\widetilde{\boldsymbol{F}}_h(\boldsymbol{x}_i) \in \mathbb{R}^{12N}$ is the force vector for the discretized system. The embedded Matlab ODE-solver `ode15s`, suitable for stiff problems, is used to solve the semi discretized problem (101). Note that the integrals in the weak formulation (93) are approximated using two point Gaussian quadrature for each interval $[S_i, S_{i+1}] \subset [0, L]$, except for the integral

$$\int_0^L \left\langle \boldsymbol{n}^e, \left[\frac{d\boldsymbol{u}}{dS} - \boldsymbol{S}(\boldsymbol{\vartheta})(\partial_S\boldsymbol{\varphi})\right] \right\rangle + \left\langle \boldsymbol{m}^e, \frac{d\boldsymbol{\vartheta}}{dS} \right\rangle dS, \tag{103}$$

which is approximated by a reduced one point Gaussian quadrature, to avoid shear locking (Simo and Vu-Quoc, 1986).

4.2. Simulation

The simulation results for a pipe with the reference length $L = 1200$ meters, semi discretized in 48 nodes, are presented in Figures 2–9. At time $t = 0$ s the pipe and the vessel is resting in its static equilibrium configuration, which is computed from (94) as $G_{\text{stat}}(\boldsymbol{\Phi}, \boldsymbol{R}_t^e; \boldsymbol{u}, \boldsymbol{\vartheta}) = 0$. After 10 second ($t = 10$ s) the system is subject to a environmental forces, taken as a linearly shared current velocity profile with surface velocity 0.8 m/s in the y direction. At $t = 30$ s a dynamic positioning controller (PID) is enabled. The objective of the controller is to move the vessel to the the reference position $(780, 0, -800)^T \in \mathbb{R}^3$. Note that the choice of origin for the spatial frame, the water surface is given by the plane $(x, y, -800)^T$, where $(x, y)^T \in \mathbb{R}^2$. The pipe configurations at $t = 0$ s, $t = 30$ s and $t = 300$ s are presented in Figure 3. Figure 4 shows that the pipe length will extend from the reference length during the simulation. The material tension forces, shown in Figure 5, indicates that tension forces will reach maximum value (upper black dots) when the vessel reaches the reference position ($t = 300$ s). For this configuration, the bending and shearing forces are presented in Figures 6–9 and the force vector fields are shown in Figures 6–7. Figures 8–9 shows the norm of the bending and shearing force vectors at the initial ($t = 0$ s) and final ($t = 300$) configurations respectively.

5. Concluding Remarks

The two objectives presented in the introductory section, that motivated this work, has been successfully achieved. Firstly, to develop a dynamic model for a freely suspended pipeline with bending stiffness suitable for simulations. The presented model is in three dimensions and model extension, sharing, twist and bending. The model is suitable for both S-lay and J-lay pipe installation as the angle of departure of the pipe from the vessel can be specified by $\boldsymbol{R}_b^t$. Secondly the pipe model was shown to be stable by a passivity check. Establishing this property is important as it enables model based controllers to be designed based on this model. High complexity controllers become more feasible

as computational power gets cheaper. However, more research should be put into investigating the numerical methods to make a faster implementation.

References

Balas, M. J., 1978. Active control of flexible systems. Journal Of Optimization Theory And Applications 25 (3), 415–436.

Braestrup, M. W., Andersen, J. B., Andersen, L. W., Bryndum, M. B., Christensen, C. J., Rishy, N., 2005. Design and Installation of Marine Pipelines. Blackwell Science Ltd, ISBN 0-6320-5984-2.

Dixon, D., Rutledge, D., February 1968. Stiffened catenary calculations in pipeline laying problem. ASME Journal of Engineering for Industry (90), 153–160.

Faltinsen, O., 1990. Sea Loads on Ships and Offshore Structures. Cambridge University Press.

Fossen, T. I., 2002. Marine Control Systems Guidence, Navigation, and Control of Ships, Rigs and Underwater Vehicles, 1st Edition. Marine Cybernetics, Trondheim Norway.

Fossen, T. I., Perez, T., 2004. Marine systems simulator (MSS). ⟨www.marinecontrol.org⟩.

Fossen, T. I., Smogeli, Ø. N., 2004. Nonlinear time-domain strip theory formulation for low-speed manoeuvering and station-keeping. Modeling, Identification and Control 25 (4), 201–221.

Guo, B., Song, S., Chacko, J., Ghalambor, A., 2005. Offshore Pipeline. Gulf Professional Publishing.

Heerema, E., 2005. Recent achievements and present trends in deepwater pipe-lay systems. In: Offshore Technology Conference.

Irvine, H. M., 1981. Cable Structures. The MIT Press.

Jensen, G. A., Transeth, A. A., Nguyen, T. D., Fossen, T. I., Jul. 2008. Modelling and control of offshore marine pipeline during pipelay. In: 17th IFAC World Congress, Seoul, South-Korea. IFAC.

Kristiansen, E., Hjulstad, A., Egeland, O., Dec. 2005. State-space representation of radiation forces in time-domain vessel models. Ocean Engineering 32 (17-18), 2195–2216.

Love, A. E. H., 1944. The Mathematical Theory of Elasticity. Dover, New York.

Martinsen, M., 1998. A finite element model for pipeline installation. Master's thesis, Stavanger University College for JP Kenny A/S.

Ogilvie, T. F., 1964. Recent progress toward the understanding and prediction of ship motions. In: Proc. Fifth Symposium on Naval Hydrodynamics, Bergen, Norway. Vol. ACR-112. ONR, pp. 3–79.

Palmer, A. C., King, R. A., 2004. Subsea Pipeline Engineering. PennWell, ISBN 1-59370-013-X.

Parinet, D., Frazer, I., 2007. J-lay and steep s-lay: Complementary tools for ultradeep water. In: Offshore Technology Conference.

Perez, T., Fossen, T. I., 2007. Kinematic models for manoeuvring and seakeeping of marine vessels. Modeling, Identification and Control 28 (1), 19–30.

Plukett, R., February 1967. Static bending stresses in catenaries and drill strings. Journal of Engineering for Industry.

Reissner, E., 1982. Some remarks on the problem of column buckling. Ingenieur-Archiv 52, 115–119.

Simo, J., Vu-Quoc, L., Oct. 1986. A three-dimensional finite-strain rod model. part II: Computational aspects. Computer Methods in Applied Mechanics and Engineering 58 (1), 79–116.

Simo, J. C., May 1985. A finite strain beam formulation. the three-dimensional dynamic problem. part I. Computer Methods in Applied Mechanics and Engineering 49 (1), 55–70.

Simo, J. C., Tarnow, N., Doblare, M., 1995. Non-linear dynamics of three-dimensional rods: Exact energy and momentum conserving algorithms. International Journal For Numerical Methods in Engineering 38, 1431–1473.

Simo, J. C., Vu-Quoc, L., Feb. 1988. On the dynamics in space of rods undergoing large motions – a geometrically exact approach. Computer Methods in Applied Mechanics and Engineering 66 (2), 125–161.

SNAME, 1950. Nomenclature for treating the motion of a submerged body through a fluid. Technical and Research Bulletin No. 1-5, 0.

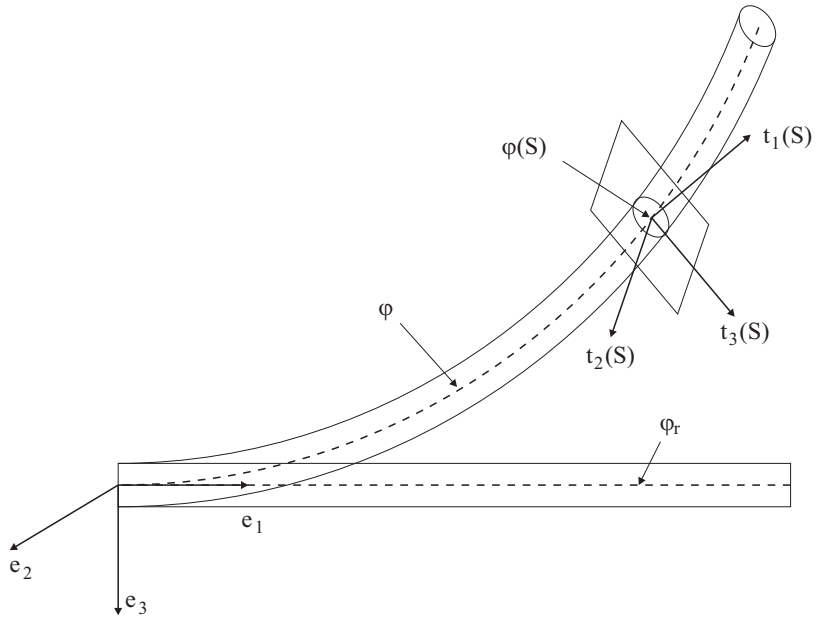

Figure 1: The pipe configuration is given by the line of centroids $\boldsymbol{\varphi}$, where the reference configuration is given as $\boldsymbol{\varphi}_r$. The cross-section of the pipe at $\boldsymbol{\varphi}(S)$ is spanned by $\boldsymbol{t}_2(S)$ and $\boldsymbol{t}_3(S)$.

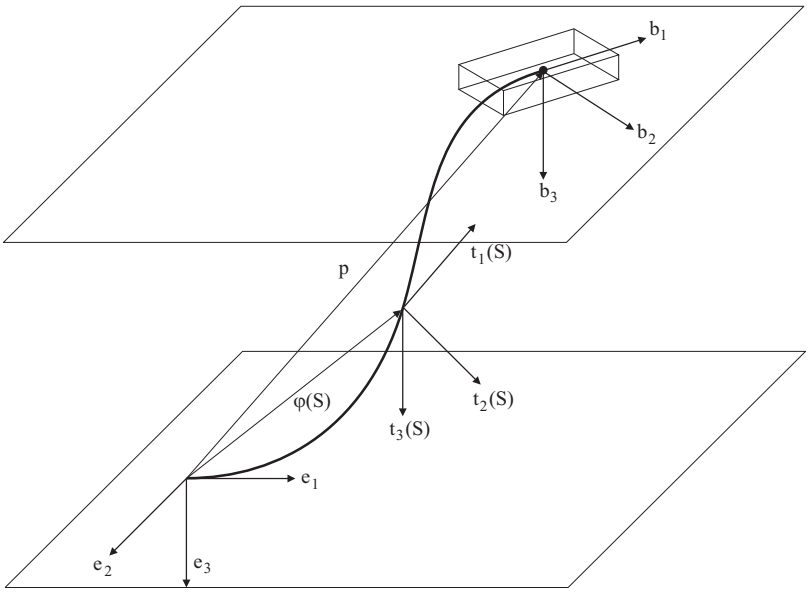

Figure 2: Illustration of an S-lay installation in three dimensions with the tree reference frames used. The position of the center of gravity of the vessel is in the spatial frame is given by $\boldsymbol{p}$.

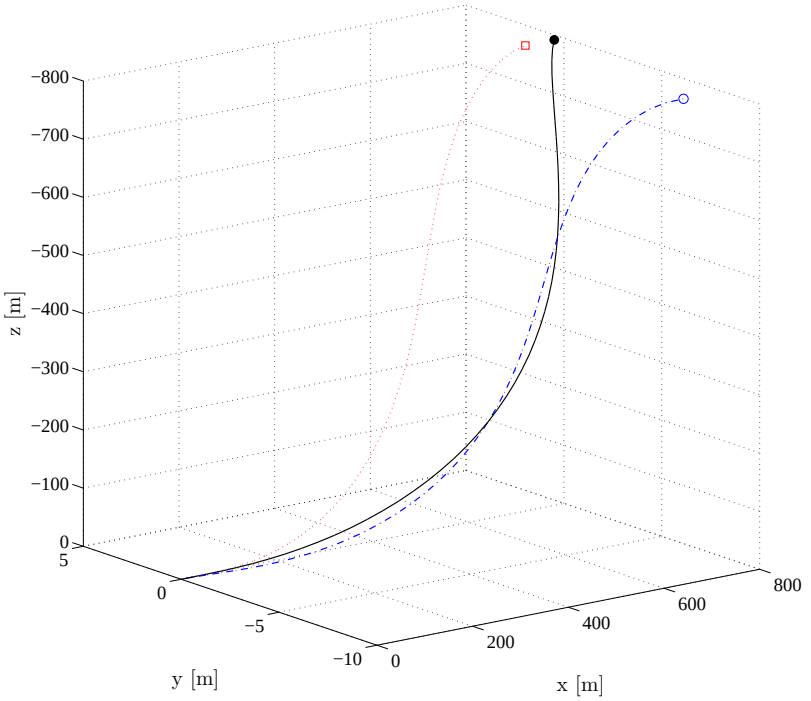

Figure 3: The initial static configuration of the pipe (red dashed line and square). The configuration after 30 s under the influence of current (blue dashed line and circle). The PID-controller is enabled at $t = 30$ s. The configuration after when the PID-controller has moved the vessel to the desired surface position (black line and solid ball).

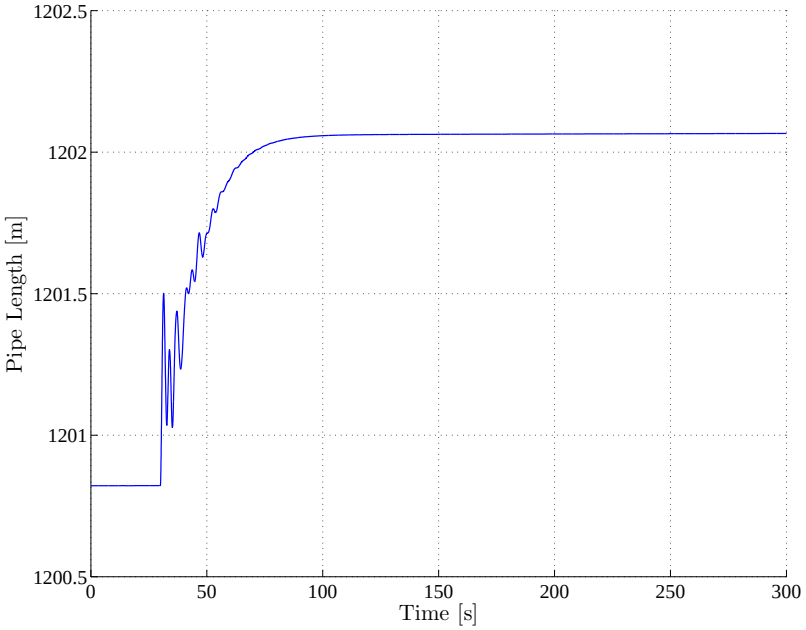

Figure 4: The pipe length, $s_h = \int_0^L |\partial_S \boldsymbol{\varphi}_h(S)|\, dS$, over the course of the 300 s simulation.

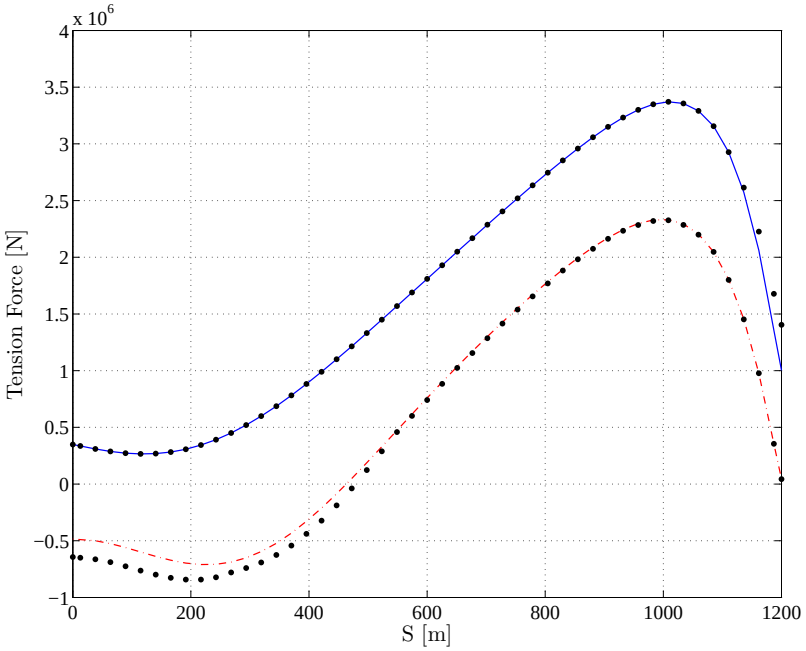

Figure 5: Material tension forces in the pipe along $\boldsymbol{t}_3$, $T_F = n^t_{h,1}$, $\boldsymbol{n}^t_h = (n^t_{h,1}, n^t_{h,2}, n^t_{h,3})^{\mathrm{T}}$. The initial tension at the time $t = 0$ (dash-dotted red line). Tension force at the time $t = 300$ seconds (blue line). Maximal and minimal tension force over the course of the simulation (black dots).

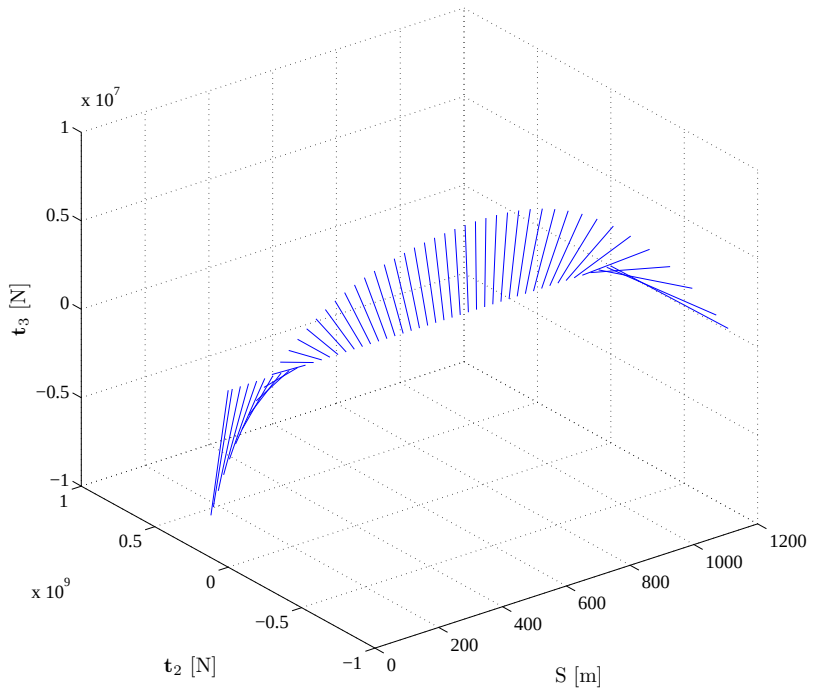

Figure 6: Bending force vector field.Bending forces, $\boldsymbol{B}_F = (m^t_{h,2}, m^t_{h,3})^{\mathrm{T}}$, $\boldsymbol{m}^t_h = (m^t_{h,1}, m^t_{h,2}, m^t_{h,3})^{\mathrm{T}}$, at the time $t = 300$ seconds.

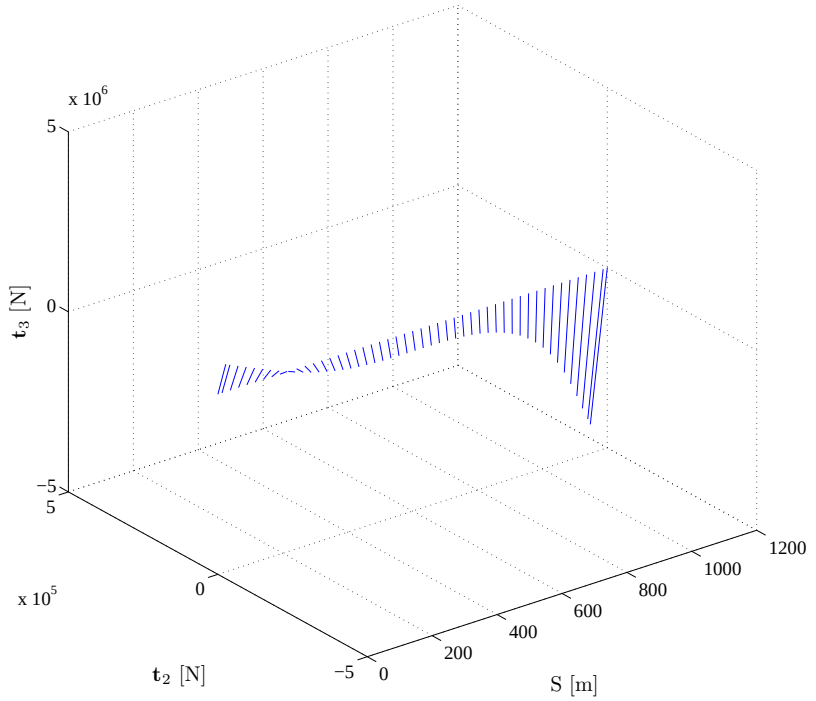

Figure 7: Shearing force vector field.Shearing forces $\boldsymbol{S}_F = (n^t_{h,2}, n^t_{h,3})^{\mathrm{T}}$, $\boldsymbol{n}^t_h = (n^t_{h,1}, n^t_{h,2}, n^t_{h,3})^{\mathrm{T}}$ at the time $t = 300$ seconds.

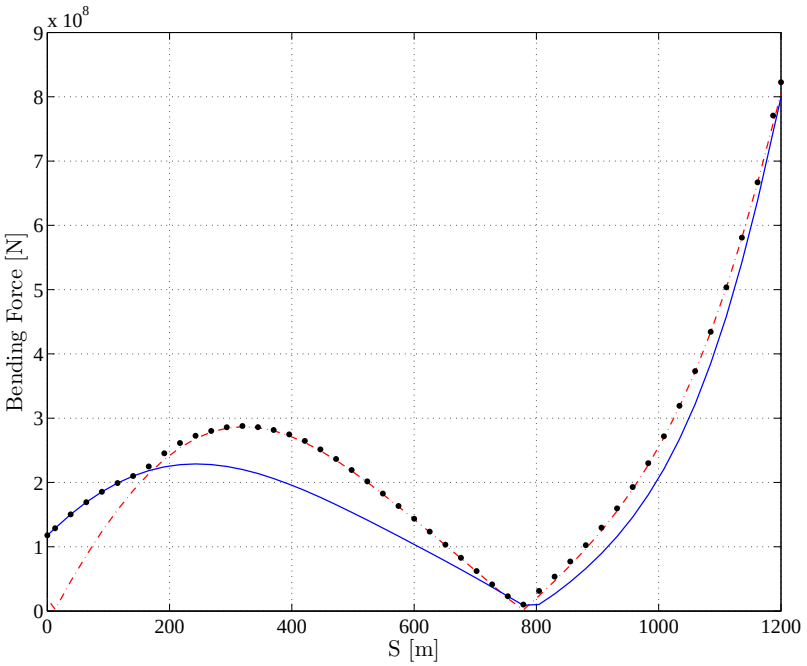

Figure 8: Bending forces, $B_F = \|(m^t_{h,2}, m^t_{h,3})^{\mathrm{T}}\|_2$, $\boldsymbol{m}^t_h = (m^t_{h,1}, m^t_{h,2}, m^t_{h,3})^{\mathrm{T}}$, in the pipe. The initial bending force at the time $t = 0$ (dash-dotted red line). Bending force at the time $t = 300$ seconds (blue line). Maximal bending force over the course of the simulation (black dots).

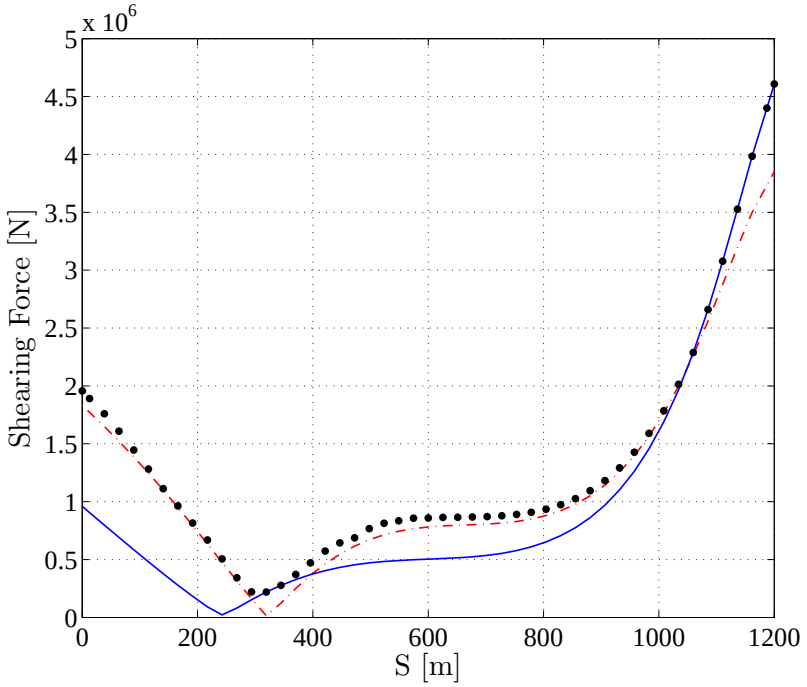

Figure 9: Shearing forces, $S_F = \|(n^t_{h,2}, n^t_{h,3})^{\mathrm{T}}\|_2$, $\boldsymbol{n}^t_h = (n^t_{h,1}, n^t_{h,2}, n^t_{h,3})^{\mathrm{T}}$, in the pipe. The initial shearing force at the time $t = 0$ (dash-dotted red line). Shearing force at the time $t = 300$ seconds (blue line). Maximal shearing force over the course of the simulation (black dots).